NJC

ROYAL SOCIETY OF CHEMISTRY

PAPER

View Article Online
View Journal | View Issue



Cite this: *New J. Chem.*, 2023, **47**, 4698

# A new mononuclear Fe(III) Mannich-base complex with selective histidine binding and catechol oxidase activity†

Bikramaditya Mandal,[a] Anwesha Haldar,[a] Rakesh Ganguly,[b] Rajat Saha *[c] and Debdas Mandal *[a]

Received 15th July 2022,
Accepted 30th January 2023

DOI: 10.1039/d2nj03501d

rsc.li/njc

The design of amino acid sensors have significant applications in biomarkers. Herein, we have developed an achiral Fe(III)-complex **[Fe$^{III}$L(bzac)]** (complex **1**) (**$H_2$L** = *N*,*N*′-dimethyl-*N*,*N*′-bi(2-hydroxy-3,5-dichlorobenzyl)-ethylenediamine (**$H_2$L**) that shows highly selective sensing of histidine over others in an aqueous methanolic solution. The complex has been synthesized by a simple stirring method using **$H_2$L** and benzylacetone (bzac) as the ancillary ligand and characterized by single crystal X-ray diffraction analysis along with other spectroscopic studies. Structural study shows that it is a simple mononuclear complex though the single molecule is chiral; however, the overall crystalline lattice is achiral in nature. In the complex, Fe(III) shows distorted octahedral geometry, and each discrete complex is connected by supramolecular hydrogen bonding interactions to form achiral 3D supramolecular structure. Both the absorption spectral analyses reveal that the complex has peaks at 484 nm due to ligand-to-metal charge transfer (LMCT) and emission spectra have a peak at 566 nm. In the presence of histidine, there is a red-shift of about 70 nm and peaks arise at about 564 nm, while the emission spectra shows that the peak at 566 nm disappears completely and a new peak at 603 nm appears. In the presence of other amino acids, there is no such distinct change in both the absorption and emission spectra of the complex. It also acts as an effective catalyst toward the oxidation of 3,5-di-*tert*-butylcatechol in methanol solvent.



## Introduction

Being an essential amino acid, histidine plays a significant role in the functions of many proteins for the growth and repair of tissues and organs.[1] Histidine also acts as the neurotransmitter or neuromodulator in muscular and central nervous system of mammals and has an important role in controlling the transmission of metal elements.[2] A persistent deficiency of histidine may cause chronic kidney diseases, Parkinson's disease, epilepsy, and pulmonary diseases, whereas excess histidine may lead to metabolic and psychological disorders.[3] Thus, the qualitative and quantitative detection and monitoring of histidine is of great importance. Different types of techniques such as electrophoresis, chemiluminescence, Raman scattering, mass spectroscopy, high performance liquid chromatography, colorimetry, and fluorimetry have been utilized for the purpose.[4] Among these, fluorimetry has gained significant attention due to its operational simplicity, high sensitivity, and real-time detection.

To date, different types of fluorescent probes such as coordination complexes, coordination polymers, and chemosensing ensembles have been developed for the highly selective detection of histidine in organic or organo-aqueous solutions. Mostly divalent metal-ion based coordination complexes or ensembles are used for the development of such sensors. Xu *et al.* have developed an ensemble of $Cu^{2+}$ with napthalimide-based fluorescent molecule that shows highly selective detection of histidine in the aqueous phase.[5] Zhao *et al.* prepared another Cu(II)-thiamine ensemble, which shows the simultaneous detection of both histidine and glutathione.[4] Li *et al.* synthesized another ensemble of Cu(II) with a trispyridine ruthenium complex for the detection of histidine.[6] Hu *et al.* have shown the turn on fluorescence of an Ir-complex $[Ir(C–N)_2(CH_3CN)_2]^+NO_3^-$ in the presence of histidine.[7] Das *et al.* reported polymeric Cu(II)-complex with phenol-based

[a] *Department of Chemistry, Sidho-Kanho-Birsha University, Purulia, 723104, West Bengal, India. E-mail: deb_mandal@yahoo.co.in*
[b] *Shiv Nadar University, NH - 91, Tehsil Dadri, Gautam Buddha Nagar, Uttar Pradesh, 201314, India*
[c] *Department of Chemistry, Kazi Nazrul University, Asansol, Paschim Bardhaman, 713340, West Bengal, India*

† Electronic supplementary information (ESI) available. CCDC 2184018(**1**). For ESI and crystallographic data in CIF or other electronic format see DOI: https://doi.org/10.1039/d2nj03501d

 

ligand (2-(((2-(phenylamino)ethyl)imino)methyl)phenol) and the resulting compound specifically senses histidine (His) with high selectivity and sensitivity under physiological conditions.[8] Chattopadhyay *et al.* observed the highly selective detection of histidine by the Cu-Schiff base complex.[9] Chan *et al.* developed another chemo-sensing ensemble using Cu and 7-*N*,*N*-diethylaminocoumarin-4-*N*-2-amino-*N*-(quinolin-8-yl)acetamide for the fluorometric detection of histidine.[10] Huang *et al.* have shown another histidine sensing ensemble of $Cu^{2+}$ with anthracene-containing chiral macrocycle.[11] In all these cases, it is supposed that histidine directly interacts with the metal center and forms the metal-histidine complex. To date, there is no example of highly selective and sensitive detection of histidine by the trivalent metal ion. In this respect, we are going to report selective histidine sensing by a Fe(III)-Mannich base complex in aqueous-methanolic solution.

Transition metal-based complexes with different types of organic ligands such as Schiff base, Mannich base, and carboxylic acids have gained much attention for their multifunctional properties such as magnetism, catalysis, sensing, antiviral, and antibacterial. Das *et al.* have reported bi-functional properties of catalysis and sensing of two different copper and manganese Schiff base complexes.[8] In another article, the same group reported the catalysis and antimicrobial activities of the copper complex.[12] Kumar *et al.* reported dual catalysis and dual sensing behavior of a copper-based metal–organic framework.[13] Following such previous instances, herein, we have investigated the bifunctional activities of complex **1**. Catechol oxidase, a copper-containing metalloenzyme, catalyzes the oxidation of a wide range of *o*-diphenols to the corresponding *o*-quinones. The generated quinones produce melanin *via* the autopolymerization process and it protects tissues from damage against pathogens and insects.[14] In 1998, the crystal structure of this metalloenzyme was determined and it was revealed that the active center consists of a hydroxo-bridged dicopper(II) center in which each Cu(II) center is coordinated to three histidine nitrogen atoms.[15] It is well established that various mono and di-copper complexes oxidize catechol to corresponding quinone.[16–19] In recent times, the catecholase activity of transition metal complexes with redox active metal ions have been explored for the development of a bioinspired catalyst.[20–27]

Herein, we report the synthesis, characterization, and bifunctional activity of a Fe(III)-Mannich-based complex **1** **[$Fe^{III}$L(bzac)]**. For the synthesis of complex **1**, *N*,*N*′-dimethyl-*N*,*N*′-bis(2-hydroxy-3,5-dichlorobenzyl)-ethylenediamine ($H_2L$) is used. Benzoylacetonate (bzac) in complex **1** plays the role of an ancillary ligand. The catecholase activity of complex **1** has been investigated following the oxidation of 3,5-di-*tert*-butylcatechol (3,5-DTBC) to 3,5-di-*tert*butylbenzoquinone (3,5-DTBQ) with molecular oxygen in methanol at 25 °C. **[$Fe^{III}$L(bzac)]** exhibits high turnover number ($K_{cat}$ = 2.5 × $10^3$) for the catalytic oxidation of 3,5-DTBC in methanol to 3,5-DTBQ. Complex **1** shows extremely selective sensing ability toward histidine (His). This study has revealed that complex **1** is more sensitive toward His compared to other amino acids. A thorough literature survey revealed that it is an interesting example of a complex capable of sensing histidine with an extensive decrease in fluorescence intensity and a large redshift (42 nm) of the excitation wavelength.

## Results and discussion

### Synthesis

A mononuclear mixed ligand complex **1** **[FeL(bzac)]** has been synthesized using facially coordinating tetradentate $N_2O_2$ ligand. Complex **1** was obtained by reacting the ligand ($H_2L$) with $FeCl_3{\cdot}6H_2O$ as the metal ion precursor and benzoylacetone as an ancillary ligand in the presence of few drops of triethylamine. The reaction is performed in methanol and the detailed strategy is summarized in Scheme 1. The IR spectra also contain all the characteristic bands of the coordinated tetradentate ligands, ($L^{2-}$). One such prominent band appears at *ca.* 1310 $cm^{-1}$ due to the $\nu$(C–O/phenolate) stretching vibrations.[28,29] Corresponding signature vibrations for the β-diketonate moiety in **1** appears in the form of a twin band at *ca.* 1590 and 1560 $cm^{-1}$ due to $\upsilon$(C═C) and $\upsilon$(C═O) stretching, respectively.[26]

### Crystal structure of the Fe(III) complex

Single crystal X-ray diffraction analysis reveals that it is a mononuclear mixed ligand complex and crystallizes in the

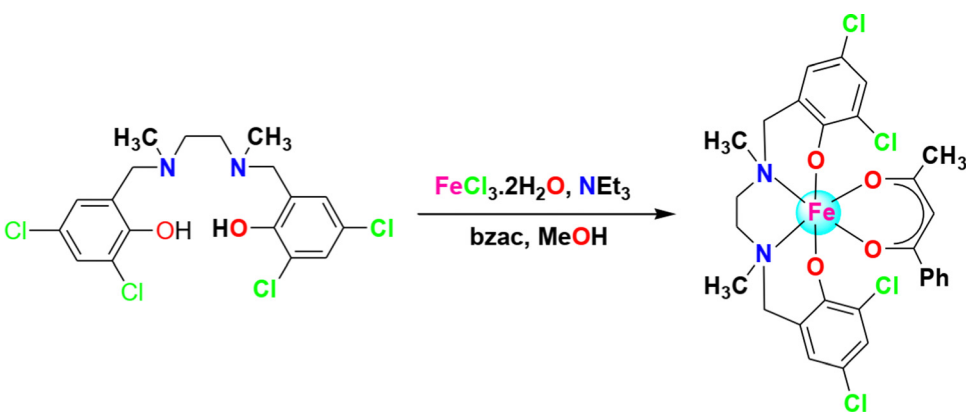


Scheme 1 Schematic presentation for the preparation of **1**.

Table 1 Crystallographic data for complex **1**

| | |
|---|---|
| Empirical formula | $C_{28}H_{27}Cl_4FeN_2O_4$ |
| Formula weight | 653.18 |
| Space group | $P2_1/n$ |
| Crystal system | Monoclinic |
| $a$, Å | 9.2164 |
| $b$, Å | 16.5872 |
| $c$, Å | 18.3092 |
| $\alpha$, deg | 90 |
| $\beta$, deg | 97.1255 |
| $\gamma$, deg | 90 |
| $V$, Å$^3$ | 2777.39 |
| $Z$ | 4 |
| $D_{calcluated}$ (g cm$^{-1}$) | 1.562 |
| $\mu$ (mm$^{-1}$) | 0.966 |
| $F$ (000) | 1340 |
| $\theta$ ranges (°) | (2.54°–27.49°) |
| Index ranges | $-11 \le h \le 110 \le k \le 21\ 0 \le l \le 23$ |
| Reflections collected | 6334 |
| $R_{int}$ | 0.0574 |
| Goodness of fit | 1.026 |
| $R1^a(F_0)$, $wR2^b(F_0)$ (all data) | 0.0405, 0.0893 |
| Largest diff. peak, deepest hole, eÅ$^{-3}$ | 0.459, −0.565 |

$^a$ $R = \sum||F_o| - |F_c||/\sum|F_o|$. $^b$ $wR = [\sum[w((F_o^2 - F_c^2)^2]/\sum w(F_o^2)^2]$.

Table 2 Selected bond distances (Å) in complex **1**

| | |
|---|---|
| Fe1–O2 | 1.9171(16) |
| Fe1–O1 | 1.9248(17) |
| Fe1–O4 | 1.9628(16) |
| Fe1–O3 | 2.0472(17) |
| Fe1–N1 | 2.2331(19) |
| Fe1–N2 | 2.263(2) |

Table 3 Selected bond angles (°) in complex **1**

| | |
|---|---|
| O2–Fe1–O1 | 95.74(7) |
| O2–Fe1–O4 | 94.39(7) |
| O1–Fe1–O4 | 98.62(7) |
| O2–Fe1–O3 | 174.60(7) |
| O1–Fe1–O3 | 89.54(7) |
| O4–Fe1–O3 | 85.97(7) |
| O2–Fe1–N1 | 95.27(7) |
| O1–Fe1–N1 | 88.59(7) |
| O4–Fe1–N1 | 167.31(7) |
| O3–Fe1–N1 | 83.65(7) |
| O2–Fe1–N2 | 88.21(7) |
| O1–Fe1–N2 | 166.83(7) |
| O4–Fe1–N2 | 93.58(7) |
| O3–Fe1–N2 | 86.38(7) |
| N1–Fe1–N2 | 78.52(7) |

centrosymmetric space group $P2_1/c$ (Table 1). The asymmetric unit contains one Fe(III), one doubly deprotonated tetradentate ligand ($L^{2-}$), and a bidentate benzoylacetonatemoiety within the crystal structure. Fe(III) shows distorted octahedral geometry. In the equatorial plane, four coordination sites are occupied by O1, O2, and N2 atoms of the ligand and O3 atom of the benzoylacetone moiety, while the axial sites are filled by N1 atoms of the ligand and O4 atoms of the bzac moiety (Fig. 1). Selected bond lengths and angles are given in Tables 2 and 3,

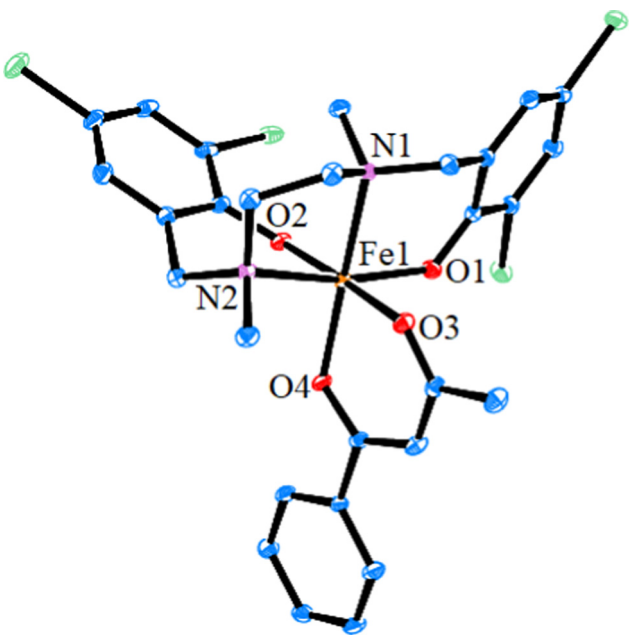


Fig. 1 ORTEP diagram of complex (**1**) with 35% ellipsoid probability (C: Blue, N: Pink, O: Red, Fe: Orange, Cl: Green).

respectively. The bond distances of Fe–N are in the range of 2.2331(19)–2.263(2) (Å) and those of Fe–O are in the range of 1.19171(16)–2.0472(17) (Å), all of which are in the desired ranges.[30,31] All the cisoid and transoid angles vary in the range of 78.52(7)–98.62(7) and 166.3(7)–174.60(7) (Å).

The Mannich base ligand shows tetradentate chelating behavior with four donor sites and it is present in the non-planar twisted form. The bzac moiety presents a planar conformation and binds the metal center in the chelating fashion with two donor oxygen atoms. Each discrete mononuclear unit is connected by C–H···Cl bonds to form 1D supramolecular zigzag chain, as shown in Fig. 2. All the hydrogen bond dimensions are given in Table 4.

## Electronic spectra of the complex

The electronic spectra of complex **1** is depicted in Fig. 3 and the main features are inscribed in the experimental section. $1 \times 10^{-4}$ M methanolic solution of **1** was used for this examination. The spectra of mononuclear octahedral complex shows a band in the 484 nm region, which can be assigned as the ligand Ph–$O^-$(pπ)-to-metal $Fe^{III}$(dπ*) charge transfer (LMCT) electronic transition.[32] The higher energy absorbances are observed at 298, 247, and 212 nm regions corresponding to intraligand n → π* and π → π* electronic transitions, respectively.[33]

## Thermogravimetric analysis

The thermogram of complex **1** was obtained by heating from 30 °C to 800 °C in $N_2$ gas atmosphere. Fe(III) complex was found to be thermally stable up to 247 °C and shows three stages decomposition up to 800 °C. Thermal decomposition proceeds with heating at 289 °C (DTGA peak at 289 °C). The first stage of

 

between a heating temperature from 247 °C to 352 °C (DTGA peak at 289 °C) corresponds to the exothermic removal of coordinated mixed ligand bzac. This stage is associated with experimental weight loss of 24% (calcd. 24.7%). The second stage occurs in the temperature range from 352 °C to 468 °C (DTGA peak at 402 °C) corresponds the exothermic removal of the coordinated 2,4-dichlorophenol group separated from the piperazinyl arm for the coordinated ligand with 14% weight loss (calcd. 13.2%). The third step continues to lose weight from 468 °C to 800 °C corresponds to the removal of remaining organic residue. The experimentally obtained weight loss associated with the DTGA peaks are in good agreement with the calculated values (Fig. 4).

### Electrochemical studies

The electrochemical behaviors of **1** have been monitored by cyclic voltammetry (CV) in acetonitrile (0.1M TBAP) using a platinum working electrode. The voltammetric features of the complex are displayed in Fig. 5. A quasi-reversible peak is obtained at $E_{1/2}$ = 0.043 V ($\Delta E_p$ = 86 mV) *vs.* saturated calomel electrode (SCE) reference with the scan rate (100 mV $s^{-1}$) corresponding to $Fe^{III}$ to $Fe^{II}$ reduction.[34]

### Interactions with amino acids

The selectivity and sensitivity of **1** with various amino acids are monitored by UV-vis and fluorescence spectroscopy. The UV-vis spectrum of complex **1** shows an important absorption band in the visible region at 484 nm. For this detection experiment, 1 μM (9 : 1, v/v, $CH_3OH : H_2O$) solution of complex **1** and 10 μM (9 : 1, v/v, $CH_3OH : H_2O$) solutions of different amino acids are prepared. With the addition of selective amino acids, the band position and the intensity are changed, as shown in Fig. 6. A new band at 511 nm with a significant redshift of 27 nm from 484 nm is observed when 1 mL solution (10 μM) of His is added to 2 mL solution (1 μM) of **1**. On the other hand, very small shifts in the band positions are observed after the addition of other amino acids in the same ratio (v/v). This study has revealed that complex **1** is more sensitive toward His compared to other amino acids. For fluorescence response, the above experiments are repeated. Only the addition of His to complex **1** shows an extensive decrease in the fluorescence intensity and a large redshift (42 nm) of excitation wavelength with $\lambda_{em}$ at 604 nm ($\lambda_{ex}$ = 511 nm), accompanied by a blueshift of excitation wavelength with $\lambda_{em}$ at 553 nm ($\lambda_{ex}$ = 511 nm) compared to the excitation wavelength of complex **1** with $\lambda_{em}$ at 562 nm ($\lambda_{ex}$ = 484 nm). The other amino acids do not produce a remarkable change in the excitation wavelength in the emission spectra, as depicted in Fig. 7.

Table 4 Hydrogen bond dimensions of complex **1**

| D–H···A | D–H/(Å) | H···A/(Å) | D···A/(Å) | <D–H···A/(°) | Symmetry |
|---|---|---|---|---|---|
| C8–H8B···O3 | 0.99 | 2.53 | 3.041(3) | 112 | |
| C10–H10A···O3 | 0.98 | 2.43 | 2.911(3) | 109 | |
| C11–H11B···Cl2 | 0.99 | 2.80 | 3.686(2) | 149 | $-1/2 + x, \frac{1}{2} - y, 1/2 + z$ |
| C27–H27···O4 | 0.95 | 2.36 | 2.703(3) | 100 | |
| C35–H35A···O3 | 0.99 | 2.36 | 2.993(3) | 121 | |

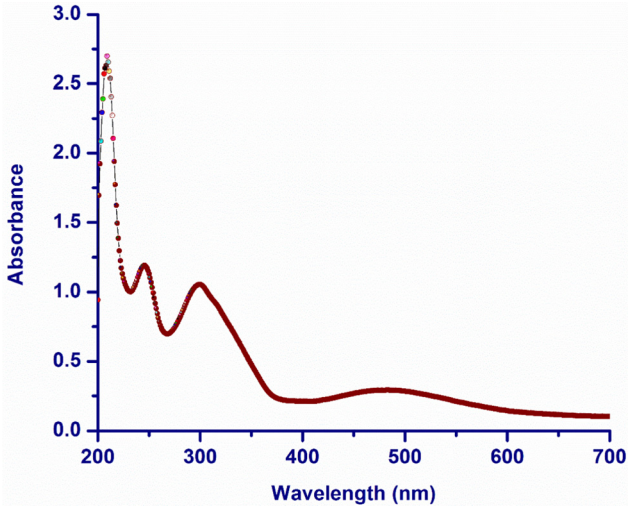


Fig. 3 Electronic absorption spectrum of **1** (1 × $10^{-4}$ M) in methanol.

### His titration experiment

The florescence response for complex **1** upon the addition of increasing amount of His is monitored by fluorescence spectroscopy, as shown in Fig. 8. For this experiment, 2 mL (1 × $10^{-5}$ M) in (9 : 1, v/v) $CH_3OH : H_2O$ solution of complex **1** is titrated with the gradual addition of 20, 40, 60, 80, 100, 120, 140, 160, 180, and 200 μL (1 × $10^{-3}$ M) in $CH_3OH : H_2O$

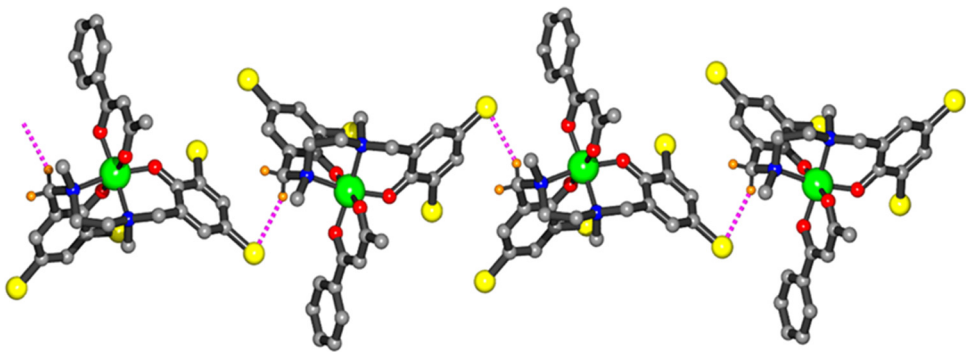

Fig. 2 1D supramolecular chain formed by C–H···Cl hydrogen bonding interactions.

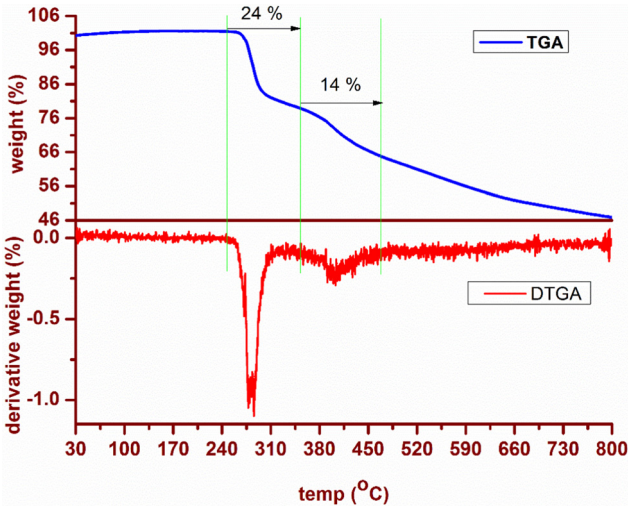


Fig. 4 TG–DTA curves for complex 1 **[Fe$^{III}$L(bzac)]**.

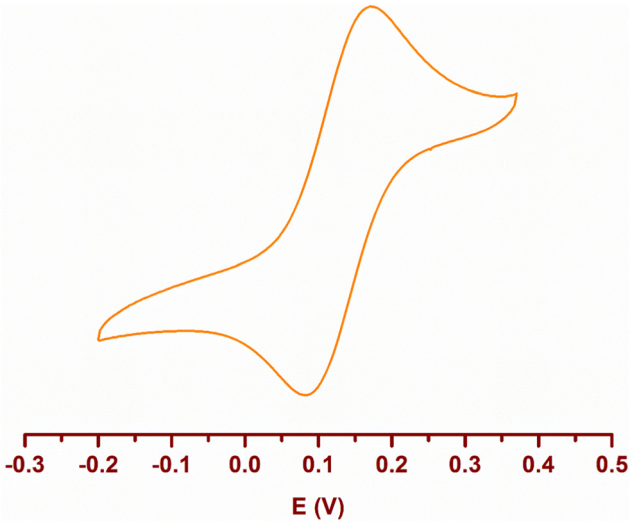


Fig. 5 Cyclic voltammogram of complex **1** ($1 \times 10^{-4}$ M) in acetonitrile with TBAP as the supporting electrolyte at 25 °C at a scan rate of 100 mV $s^{-1}$.

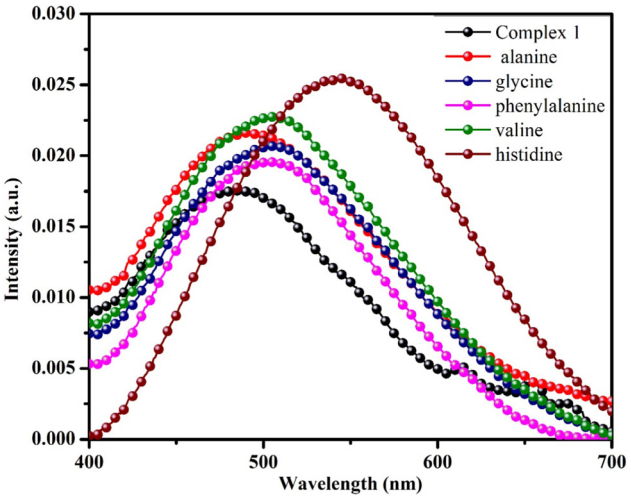


Fig. 6 UV-Vis absorbance spectra of complex **1** (1 μM) with amino acids (10 μM) in (9 : 1, v/v) $CH_3OH : H_2O$.

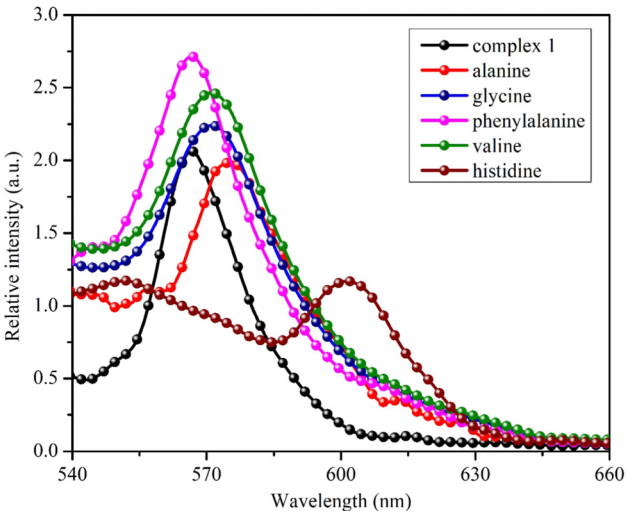


Fig. 7 Fluorescence spectra of complex **1** (1 μM) with amino acids (10 μM) in (9 : 1, v/v) $CH_3OH : H_2O$.

(9 : 1, V/V) solution of His. This experiment shows a gradual increase in the intensity of the emission spectra of His in both blueshift and redshift regions at about 553 and 604 nm, respectively. Fig. 9 further implies a linear enhancement of the fluorescence response of the titration experiment in the range of 20 to 200 μL of ($1 \times 10^{-3}$ M) solution of His for the linear enhancement of fluorescence response at 604 and 553 nm, respectively. The linear regression equation is $Y = 0.06181$ [His] $\times 10^{-5}$ (M) + (−0.24431) with correlation coefficient $R^2 = 0.99308$ and $Y = 0.12696$ [His] $\times 10^{-5}$ (M) + (−1.87267) with correlation coefficient $R^2 = 0.98764$ for the linear enhancement of fluorescence response at 604 and 553 nm, respectively.

### Catalytic oxidation of 3,5-DTBC

The catecholase activity of **1** was studied using 3,5-di-*tert*-butyl catechol (3,5-DTBC) as a model substrate in methanol under aerobic conditions at room temperature. The most widely used 3,5-DTBC has been used as the substrate as it can be easily oxidized to 3,5-di-*tert*-butyl benzoquinone (3,5-DTBQ). The two bulky substutuents on the catechol ring makes it easily oxidizable to the corresponding *o*-quinone 3,5-DTBQ and at the same time, bulky *tert*-butyl methyl substituent's prevent further oxidation reactions. To monitor the reaction, $6.5 \times 10^{-4}$ M metabolic solutions of **1** were added with 100 equivalents of 3,5-DTBC. After mixing 3,5-DTBC into complex **1**, sequentially, the progress of the reaction was recorded by the UV-vis spectra of the mixtures at 5 min time intervals. The time-resolved spectra for the conversion of 3,5-DTBC to 3,5-DTBQ (quinone band maxima) was observed at a wavelength of about 400 nm in methanol, as shown in Fig. 10. The rate constant for a particular complex–substrate concentration ratio was obtained by the change in the absorbance *versus* time plot by employing the initial rate method. The substrate concentration dependence of

 

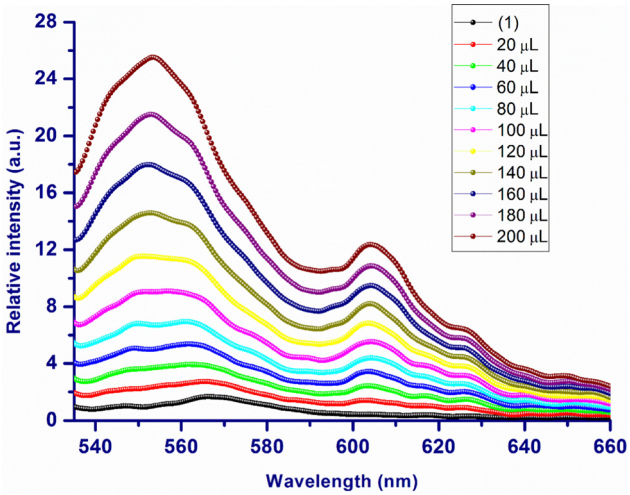


Fig. 8 The fluorescence spectra of **1** (0.1 μM) with the addition of increasing concentration of His (10 μM) in $CH_3OH : H_2O$ (9 : 1, V/V).

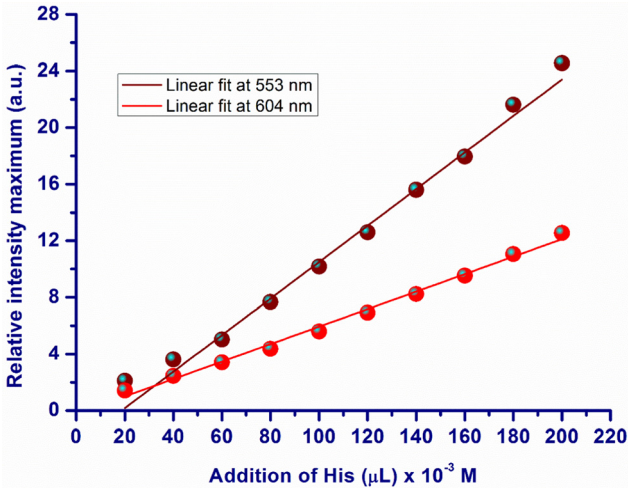


Fig. 9 The linear relationship between the fluorescence increment of complex **1** with His.

the oxidation rate was examined under aerobic conditions, using $6.5 \times 10^{-4}$ M solutions of **1** and increasing amounts of 3,5-DTBC from $1.5 \times 10^{-3}$ M to $5 \times 10^{-3}$ M. The observed rate *vs.* [substrate] plot in methanol solution, as well as Lineweaver–Burk plot, is given in Fig. 11. The observed rate *versus* substrate concentration data were, then analyzed on the basis of the Michaelis–Menten approach of the enzymatic kinetics to determine the Michaelis–Menten constant ($K_M$) and maximum initial rate ($V_{max}$) using Michaelis–Menten plots and Lineweaver–Burk plots. $K_{cat}$ were obtained by dividing the $V_{max}$ values by the concentration of the corresponding complexes. Table 5 shows the catecholase activities of the reported mononuclear Fe complexes. It is notable that complex **1** exhibits very high turnover number ($K_{cat} = 2.5 \times 10^3$ $h^{-1}$) for the catalytic oxidation of 3,5-DTBC in methanol to 3,5-DTBQ as compared to several reported mononuclear Fe complexes.

A plausible complex–substrate intermediates in the catalytic cycles is shown in Scheme 2. We have checked the ESI-MS

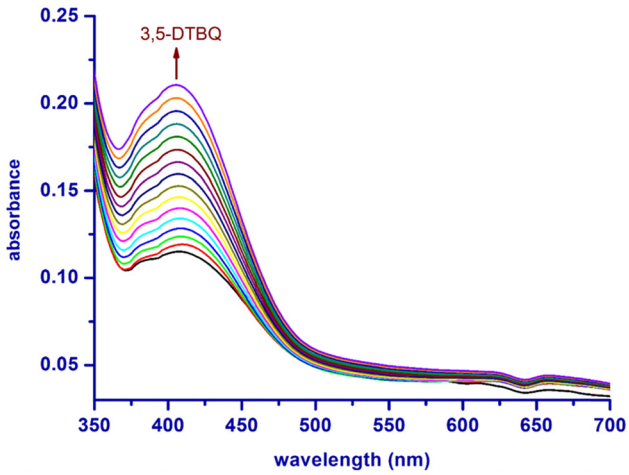


Fig. 10 3,5-DTBQ spectra at 5 min time intervals at 402 nm after the addition of 10 equiv. of 3,5-DTBC to a $6.5 \times 10^{-4}$ M methanol solution of **1**.

spectra for complex **1** after 15 min of mixing of complex **1** and 3,5-DTBC with 1 : 10 mole ratio in methanol (Fig. S1, ESI†). The observed ESI-MS features for the resulting mixture of complex **1** with 3,5-DTBC shows characteristic peaks at $m/z$ = 243, 301, 413, 463, 555, and 712. The signal at about $m/z$ = 243 is due to the formation of $[3,5\text{-DTBC(Na)}]^+$, a sodium aggregate of quinone. The peak at $m/z$ = 463 can be assigned to the 2 : 1 quinone sodium aggregate $[(3,5\text{-DTBC})_2Na]^+$. Another peak at $m/z$ = 555 is possibly due to the formation of a sodium aggregate of the intermediate species $[Fe^{III}(L)(CH_3OH)_2H]^+$. The formation of a sodium aggregate of the intermediate species $[Fe^{III}(L)(3,5\text{-DTBC})Na]^+$ is confirmed by the peak at $m/z$ = 712.

The formation of $H_2O_2$ during the catalytic oxidation of 3,5-DTBC to 3,5-DTBQ by complex **1** indicates some idea related to probable mechanisms involved in the catalytic processes. Complex **1** give a positive result to the formation $H_2O_2$ as the byproduct by observing the characteristic peak of $I^{3-}$ at 353 nm, produced by the reaction of generated peroxide with potassium iodide. 80% $H_2O_2$ have been produced with respect to the formation of 3,5-DTBQ after 1 h oxidation of 3,5-DTBC and this phenomenon suggests that the two-electron reduction of molecular oxygen occurred during the catalytic cycle. A probable mechanistic cycle for the oxidation of 3,5-DTBC to 3,5-DTBQ catalyzed by complex **1** in the presence of air is shown Scheme 2. In the first step of the catalytic cycle, complex **1** dissociates to produce active species **1a**. The active species then binds with 3,5-DTBC to form **1b** species. Then, the reaction proceeds through the formation of the Fe(II)-semiquinonate radical species **1c**. In the final step of the catalytic cycle, Fe(II)-semiquinonate species **1** reacts with di-oxygen to produce 3,5-DTBQ along with the regeneration of complex **1** and $H_2O_2$ as the byproduct.

## Experimental

### Materials

The tetradentate ligand *N*,*N*′-dimethyl-*N*,*N*′-bis(2-hydroxy-3,5-dichlorobenzyl)-ethylenediamine (**$H_2$L**) was reproduced by

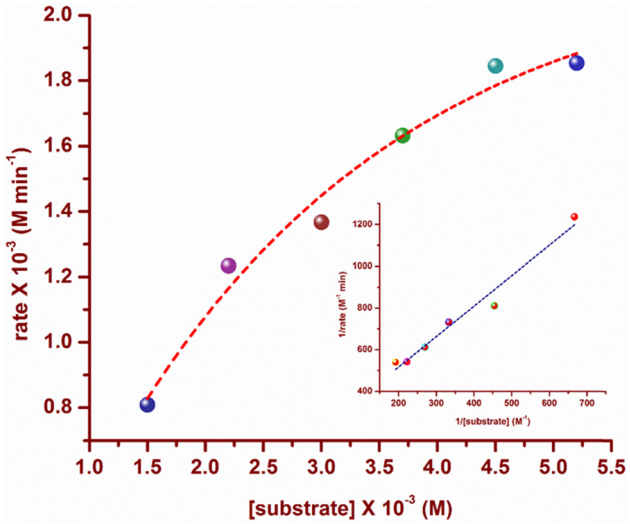


Fig. 11 Plot of rate *vs.* [substrate] in the presence of (**1**) in methanol; the inset represents the Lineweaver–Burk plot.

earlier reported method.[37] Solvents were reagent grade, purified using appropriate drying agents, and distilled under nitrogen prior to their use.[38] All other reagents were commercially available and were of reagent grade and used as received without further purification.

Caution! Perchlorate compounds are potentially explosive. Only a small amount of material should be prepared and handled with care.

### Preparation of complex 1 [$Fe^{III}$L(bzac)]

0.14g (0.5 mmol) $FeCl_3{\cdot}6H_2O$ was added to the methanolic solution of 0.22 g (0.5 mmol) $\mathbf{H_2L}$. The mixture was stirred for 30 min and 0.08 g (0.5 mmol) benzoylacetone was added. A few drops of triethylamine were added to the solution. The resulting solution was refluxed for 1 h. A dark brown color solution was obtained and filtered. The filtrate was kept in open air for crystallization. A brown crystalline compound was obtained and collected. Finally, a crystalline compound along with some diffraction quality crystals were obtained and collected by filtration. Yield: 0.18 g (55%), Anal. Calcd. for $C_{28}H_{27}Cl_4N_2O_4Fe$: C, 51.45; H, 4.13; N,4.28. Found: C, 51.05; H, 4.44; N,4.82. IR (KBr disk, $cm^{-1}$): 3416, 1590, 1557, 1454, 1360, 1317, 1177, 759. UV-vis ($CH_3OH$) [$\lambda_{max}$/nm ($\varepsilon$/$mol^{-1}$ $cm^2$)]: 299 (6615), 484 (2112).

### Physical measurements

UV-Visible spectra for complex **1** in solutions were recorded on a PerkinElmer 950 UV/VIS/NIR spectrophotometer, while for the infrared spectra, a Nicolet Magna 750 FT-IR spectrometer series II was employed with samples prepared as KBr pellets. Fluorescence spectral studies were done on a PerkinElmer LS 55 FL spectrophotometer using a 450 W Xenon (Xe) lamp as the excitation source. All spectral data were recorded at 25 °C. Fluorescence measurements are done using 1 cm quartz cells with 10 nm slit width for emission experiments. Thermogravimetric (TG) analysis was performed using a PerkinElmer S.N.5032010 instrument.

### X-Ray crystallography

Diffraction quality crystals of **1** were grown at room temperature by the slow diffusion of methanolic reaction mixture. The intensity data for complex **1** was measured on a Bruker SMART 1000 CCD diffractometer using graphite monochromated Mo Kα radiation ($\lambda$ = 0.71073 Å) at 293 K. Intensity data were collected with $\theta_{max}$ of 24.99°. Relevant crystal data and refinement details are given in Table 1. No crystal decay was observed during the data collections for (**1**). The structures of the entitled complex were solved by direct methods[39] and refined on $F^2$ by a full-matrix least-squares procedure[40] using the SHELXL 97 program.

### Catecholase activity

The catecholase activity of **1** was explored employing the most familiar substrate 3,5-DTBC as a model substrate in methanol under aerobic conditions at room temperature.[41] To examine the catecholase activity of (**1**), a 6.5 × $10^{-4}$ M solution of (**1**) in methanol was mixed with 10 equiv. of 3,5-DTBC under the specified conditions. The reaction was performed spectrophotometrically by scrutinizing the increase in the maximum absorbance of the quinone band at about 400 nm against time.[42] The absorbance *vs.* wavelength spectra of the solution was recorded at regular time intervals of 5 min. It is noteworthy that a blank experiment without complex (**1**), up to 6 h in methanol, does not show any quinone band at about 400 nm.

Table 5 Kinetics parameters for several mononuclear Fe(III) complexes

| Complex | Solvent | $V_{max}$ (M $min^{-1}$) | $K_M$ (M) | $K_{cat}$ ($h^{-1}$) | Ref. |
|---|---|---|---|---|---|
| $[Fe(L^1)_2]SCN$ | ACN | 9.12× $10^{-6}$ | 13.37 × $10^{-4}$ | 5.52 | 35 |
| $[Fe(L^2)(HL^3)]ClO_4$ | ACN | 4.178× $10^{-5}$ | 134.05 × $10^{-4}$ | 25.07 | 35 |
| $[Fe(L^4)(phen)]$ | MeOH | 6.847 × $10^{-4}$ | 2.146 × $10^{-4}$ | 339 | 36 |
| $[Fe(L^4)(bipy)]$ | MeOH | 3.315 × $10^{-4}$ | 2.142 × $10^{-4}$ | 352 | 36 |
| $[Fe(L^5)(phen)]$ | MeOH | 5.407 × $10^{-4}$ | 2.330 × $10^{-4}$ | 444 | 36 |
| $[Fe(L^5)(bipy)]$ | MeOH | 6.969 × $10^{-4}$ | 3.013 × $10^{-4}$ | 474 | 36 |
| **[$Fe^{III}$L(bzac)] (1)** | MeOH | 4.44(2) × $10^{-3}$ | 6.64 × $10^{-3}$ | 2.5 × $10^3$ | This work |

where, $HL^1$ = 1-((3-amino-2,2-dimethylpropylimino)methyl)naphthalen-2-ol, $\mathbf{H_2L^2}$ = *N*,*N*′-bis(3-ethoxysalicylidene)2,2-dimethyl-1,3-propanediamine, $HL^3$ = 2-((3-amino-2,2-dimethylpropylimino)methyl)-6-ethoxyphenol, $H_3L^4$ = bis(5-(*tert*-butyl)-2-hydroxybenzyl)glycine, and $H_3L^5$ = bis(2-hydroxy-5-methylbenzyl)glycine.

 

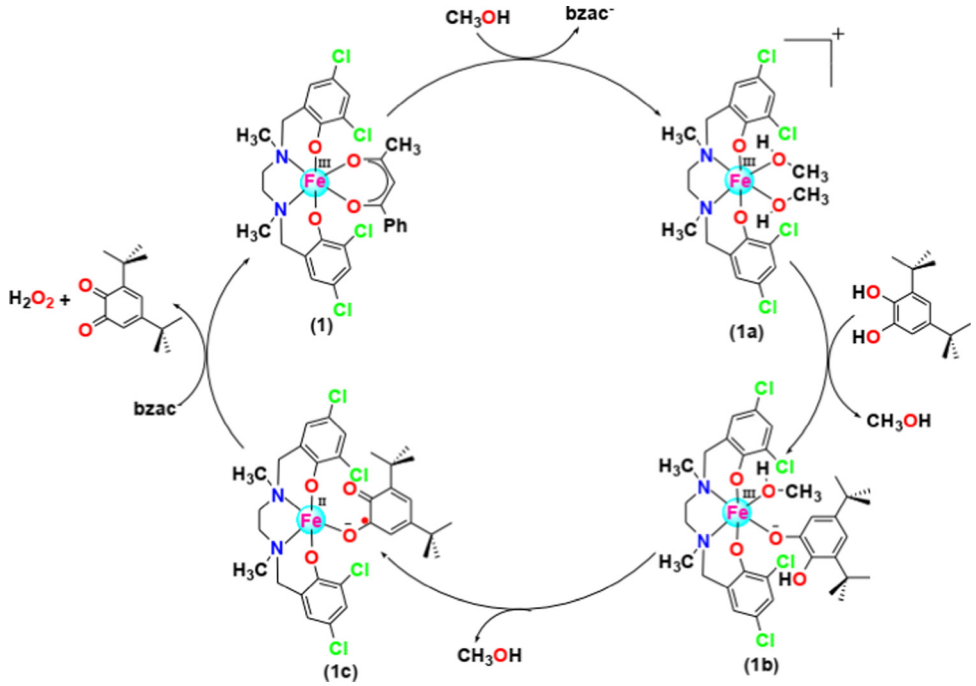


Scheme 2 A plausible mechanistic pathway for the aerobic catechol oxidation catalyzed by complex **1**.

### Detection of hydrogen peroxide

The detection of $H_2O_2$ was accomplished by the modified iodometric method during catalytic reactions.[43] The reaction mixture containing complex (**1**) and 3,5-DTBC in methanol was employed for the detection process. After 1 h of reaction, an equal volume of distilled water was included in the reaction mixture. One of the reaction products, quinone, was extracted from the mixture using DCM. A few drops of conc. $H_2SO_4$ were added to the aqueous extract to cease further oxidation. 1 mL KI (10% solution) and three drops of ammonium molybdate (3% solution) were added to the aqueous reaction mixture. $H_2O_2$ produced from catalytic reaction oxidizes $I^-$ to $I_2$. In the presence of excess iodide ions, the triiodide ion was formed according to the reaction, $I_2 + I^- \rightarrow I_3^-$. The reaction rate surges with increasing concentrations of acid ($H_3O^+$) and the inclusion of ammonium molybdate solution almost immediately condenses the reaction. The formation of $I_3^-$ was detected spectrophotometrically owing to the development of the characteristic $I_3^-$ band.

## Conclusion

Mononuclear mixed ligand octahedral Fe(III) complex was prepared using sterically constrained phenol-based ligand *N*,*N*′-dimethyl-*N*,*N*′-bis(2-hydroxy-3,5dichlorobenzyl)-ethylenediamine (**$H_2L$**) and benzoyl acetone as a co-ligand. Complexes were characterized by a single crystal X-ray diffractometer as well as other spectroscopic tools. The resulting complex exhibits catechol oxidase activity with high turnover number number ($K_{cat} = 2.5 \times 10^3\ h^{-1}$). The oxidation reaction proceeds through the formation of the Fe(II)-semiquinonate radical species. The selectivity of complex **1** with various amino acids was monitored by UV-vis and fluorescence spectroscopy. The study revealed that complex **1** was more sensitive toward His compared to other amino acids. Absorption spectral analyses show that in the presence of His, the band position and intensity of the electronic spectra of the complex **1** are significantly changed. The addition of His to complex **1** gives an extensive decrease in the fluorescence intensity and a large redshift (42 nm) in the excitation wavelength.

## Conflicts of interest

There are no conflicts to declare.

## Acknowledgements

Financial support received from Department of Science and Technology, Government of West Bengal, Kolkata (Project memo no. 1071(Sanc)/ST/P/S&T/15G-4/2015 dated 23.02.2016) is gratefully acknowledged. We are grateful for the instrumental support from Department of Inorganic Chemistry, Indian Association for the Cultivation of Science.

## References

1 (*a*) L. D. S. Johnson, H. A. Goubran and R. R. Kotb, *Anticancer Res.*, 2014, **34**, 593; (*b*) K. Jung, L. Fried, S. Behr and R. Heermann, *Curr. Opin. Microbiol.*, 2012, **15**, 118.

2 (*a*) H. L. Haas, O. A. Sergeeva and O. Selbach, *Physiol. Rev.*, 2008, **88**, 1183; (*b*) Y. Kusakari, S. Nishikawa, S.-I. Ishiguro and M. Tamai, *Curr. Eye Res.*, 1997, **16**, 600; (*c*) G. N. Chen, X. P. Wu, J. P. Duan and H. Q. Chen, *Talanta*, 1999, **49**, 319.

3 (*a*) A. L. Jones, M. D. Hulett and C. R. Parish, *Immunol. Cell Biol.*, 2005, **83**, 106; (*b*) M. Watanabe, M. E. Suliman, A. R. Qureshi,E. Garcia-Lopez, P. Bárány, O. Heimbürger, P. Stenvinkel and B. Lindholm, *Am. J. Clin. Nutr.*, 2008, **87**, 1860.
4 N. Pengjuan, J. Dafeng, C. Chuanxia, J. Yuanyuan, L. Yizhong and Z. Zhenlu, *Analyst*, 2018, **143**, 4442.
5 H. I. Un, S. Wu, C. B. Huang, Z. Xu and L. Xu, *Chem. Commun.*, 2015, **51**, 3143.
6 Y. Yang, Y. Li, X. Zhi, Y. Xu and M. Li, *Dyes Pigm.*, 2020, **183**, 108690.
7 H. Wang, B. Xu, H. Chen, D. Li, X. Shen, F. Cai, Y. Xu, L. Zhou and L. Hu, *Inorg. Chim. Acta*, 2020, **511**, 119799.
8 B. Kumari, S. Kundu, K. Ghosh, M. Banerjee, S. K. Pradhan, S. M. Islam, P. Brandão, V. Félix and D. Das, *Dalton Trans.*, 2018, **47**, 14008.
9 A. Mondal, C. Das, M. Corbella, A. Bauzá, A. Frontera, M. Saha, S. Mondal, K. D. Saha and S. K. Chattopadhyay, *New J. Chem.*, 2020, **44**, 7319.
10 Q. H. You, A. W. M. Lee, W. H. Chan, X. M. Zhua and K. C. Leung, *Chem. Commun.*, 2014, **50**, 6207.
11 X. Huang, K. Li, X. Wang and P. Xia, *Spectrochim. Acta, Part A*, 2018, **205**, 287.
12 S. Adhikari, S. Lohar, B. Kumari, A. Banerjee, R. Bandopadhyay, J. S. Matalobos and D. Das, *New J. Chem.*, 2016, **40**, 10094.
13 R. Saha, B. Joarder, A. Singha Roy, S. M. Islam and S. Kumar, *Chem. – Eur. J.*, 2013, **19**, 16607.
14 W. S. Pierpoint, *Biochem. J.*, 1969, **112**, 609–616.
15 T. Klabunde, C. Eicken, J. C. Sacchettini and B. Krebs, *Nat. Struct. Biol.*, 1998, **5**, 1084–1090.
16 I. A. Koval, D. Pursche, A. F. Stassen, P. Gamez, B. Krebs and J. Reedijk, *Eur. J. Inorg. Chem.*, 2003, 1669.
17 I. A. Koval, M. Huisman, A. F. Stassen, P. Gamez, O. Roubeau, C. Belle, J. L. Pierre, E. Saint-Aman, M. Lüken, B. Krebs, M. Lutz, A. L. Spek and J. Reedijk, *Eur. J. Inorg. Chem.*, 2004, 4036.
18 A. Banerjee, S. Sarkar, D. Chopra, E. Colacio and K. K. Rajak, *Inorg. Chem.*, 2008, **47**, 4023.
19 B. Mandal, M. C. Majee, T. Rakshit, S. Banerjee, P. Mitra and D. Mandal, *J. Mol. Struct.*, 2019, **1193**, 265.
20 S. Adhikari, A. Banerjee, S. Nandi, M. Fondo, J. Sanmartín-Matalobos and D. Das, *RSC Adv.*, 2015, **5**, 10987.
21 S. K. Dey and A. Mukherjee, *New J. Chem.*, 2014, **38**, 4985.
22 M. Mitra, A. K. Maji, B. K. Ghosh, P. Raghavaiah, J. Ribas and R. Ghosh, *Polyhedron*, 2014, **67**, 19.
23 D. Mondal, S. Kundu, M. C. Majee, A. Rana, A. Endo and M. Chaudhury, *Inorg. Chem.*, 2017, **56**, 9448.
24 P. Chakraborty, S. Majumder, A. Jana and S. Mohanta, *Inorg. Chim. Acta*, 2014, **410**, 65.
25 A. Guha, K. S. Banu, A. Banerjee, T. Ghosh, S. Bhattacharya, E. Zangrando and D. Das, *J. Mol. Catal. A: Chem.*, 2011, **338**, 51.
26 B. Mandal, T. Chakraborty, I. Ali, D. Mondal, M. C. M. C. Majee, S. Raha, K. Ghosh, P. Mitra and D. Mandal, *J. Indian Chem. Soc.*, 2017, **94**, 1079.
27 B. Mandal, M. C. Majee, D. Mandal and R. Ganguly, *J. Mol. Struct.*, 2020, **1202**, 127340.
28 D. Mandal, S. M. T. Abtab, A. Audhya, E. R. T. Tiekink, A. Endo, R. Clérac and M. Chaudhury, *Polyhedron*, 2013, **52**, 355.
29 D. Mandal, P. B. Chatterjee, S. Bhattacharya, K.-Y. Choi, R. Clérac and M. Chaudhury, *Inorg. Chem.*, 2009, **48**, 1826.
30 M. Scarpellini, A. Neves, A. J. Bortoluzzi, I. Vencato, V. Drago, W. A. Ortizc and C. Zuccod, *J. Chem. Soc., Dalton Trans.*, 2001, 2616.
31 P. Angaridis, J. W. Kampf and V. L. Pecoraro, *Inorg. Chem.*, 2005, **44**, 3626.
32 S. I. Lo, J. W. Lu, W. J. Chen, S. R. Wang, H. H. Wei and M. Katada, *Inorg. Chim. Acta*, 2009, **362**, 4699.
33 A. Dutta, S. Biswas, M. Dolai, B. K. Shaw, A. Mondal, S. K. Saha and M. Ali, *RSC Adv.*, 2015, **5**, 23855.
34 M. Velusamy, R. Mayilmurugan and M. Palaniandavar, *Inorg. Chem.*, 2004, **43**, 6284.
35 T. Basak, K. Ghosh, C. J. Gómez-García and S. Chattopadhyay, *Polyhedron*, 2018, **146**, 42.
36 S. Indira, G. Vinoth, M. Bharathi, S. Bharathi, A. Kalilur Rahiman and K. Shanmuga Bharathi, *Inorg. Chim. Acta*, 2019, **495**, 118988.
37 B. Mandal, A. Haldar, R. Saha and D. Mandal, *J. Mol. Struct.*, 2020, **1220**, 128723.
38 D. D. Perrin, W. L. F. Armarego and D. R. Perrin, *Purification of Laboratory Chemicals*, 1980.
39 G. M. Sheldrick, *Acta Crystallogr., Sect. A: Found. Crystallogr.*, 1990, **46**, 467.
40 G. M. Sheldrick, *J. Phys. Chem.*, 1993, **98**, 9700.
41 J. Mukherjee and R. Mukherjee, *Inorg. Chim. Acta*, 2002, **337**, 429.
42 F. Zippel, F. Ahlers, R. Werner, W. Haase, H.-F. Nolting and B. Krebs, *Inorg. Chem.*, 1996, **35**, 3409.
43 M. Das, R. Nasani, M. Saha, S. M. Mobin and S. Mukhopadhyay, *Dalton Trans.*, 2015, **44**, 2299.

 